Nano Energy 82 (2021) 105680

Contents lists available at ScienceDirect

Nano Energy

journal homepage: http://www.elsevier.com/locate/nanoen

# Artificial tactile peripheral nervous system supported by self-powered transducers

Libo Chen [a], Chenyu Wen [a], Shi-Li Zhang [a], Zhong Lin Wang [a,b,c], Zhi-Bin Zhang [a,*]

[a] Division of Solid State Electronics, Department of Electrical Engineering, Uppsala University, Uppsala 75121, Sweden
[b] Beijing Institute of Nanoenergy and Nanosystems, Chinese Academy of Sciences, Beijing 100083, China
[c] School of Material Science and Engineering, Georgia Institute of Technology, Atlanta, GA 30332, USA

ARTICLE INFO

*Keywords:*
Triboelectric nanogenerator
Electronic skin
Slowly adapting type I afferent
Artificial tactile nervous system

ABSTRACT

The tactile peripheral nervous system innervating human hands, which is essential for sensitive haptic exploration and dexterous object manipulation, features overlapped receptive fields in the skin, arborization of peripheral neurons and many-to-many synaptic connections. Inspired by the structural features of the natural system, we report a supersensitive artificial slowly adapting tactile afferent nervous system based on the triboelectric nanogenerator technology. Using tribotronic transistors in the design of mechanoreceptors, the artificial afferent nervous system exhibits the typical adapting behaviours of the biological counterpart in response to mechanical stimulations. The artificial afferent nervous system is self-powered in the transduction and event-driven in the operation. Moreover, it has inherent proficiency of neuromorphic signal processing, delivering a minimum resolvable dimension two times smaller than the inter-receptor distance which is the lower limit of the dimension that existing electronic skins can resolve. These results open up a route to scalable neuromorphic skins aiming at the level of human's exceptional perception for neurorobotic and neuroprosthetic applications.

## 1. Introduction

A tactile afferent nervous system is essential to achieving the human capability in haptic exploration, tender touching, proprioception and dexterous object manipulation. Therefore, electronic skins (e-skins) innervated with an artificial afferent nervous system are indispensable for emerging anthropomorphic neurorobotics and neuroprosthetics [1–3]. A tactile signal provides direct mechanical information about the interaction between skin (in particular fingertips) and object. This directness facilitates rapid planning and sensorimotor control during object manipulation, in contrast to, e.g. visual afferents that produce indirect information about such an interaction [4–7]. The extraordinary tactile perception and the rapid sensorimotor reactions are largely ascribed to the distributed, parallel and event-driven computation based on spatiotemporal spike train (action potentials) in a biological nervous system. This distributed parallelism is much more efficient in signal processing for solving complex real-world problems than sequential and centralized operations defined by the classical von Neumann computer architecture [8].

Most previous efforts in the e-skin development focus on distal individual sensors and sensor arrays [9–15]. Few experimental attempts encompass artificial tactile nerves [16,17]. Pioneering studies in mimicking the function of an afferent-innervated skin mostly use two-dimensional (2D) tactile sensor arrays interfaced with complicated readout circuits. Individual tactile sensors are then sampled sequentially and periodically to map the force distribution [18]. With this approach, the readout latency and power consumption increase with the number of tactile sensors. It renders the artificial skin difficult to be scaled up for real neurorobotic and neuroprosthetic applications. The serial readout scheme prevents artificial skin from responding properly to highly dynamic stimuli. Such dynamic stimulations occur when fingertips with fingerprints on the surface touch and slide on an object. The proper response to dynamic stimulations is important for human to perceive and extract physical properties like roughness and hardness of the object. The spatial resolution of force mapping reconstructed from data readout is usually limited by the inter-sensor distance in the sensor array. It is worth noting that the human fingertip can discriminate spatial tactile details down to the nanometre scale [19]. As a comparison, the mechanoreceptors in the fingertip are typically tens of micrometres in size and the inter-mechanoreceptor distance is at tens to

* Corresponding author.
*E-mail address:* zhibin.zhang@angstrom.uu.se (Z.-B. Zhang).

https://doi.org/10.1016/j.nanoen.2020.105680
Received 31 October 2020; Received in revised form 27 November 2020; Accepted 8 December 2020
Available online 13 December 2020

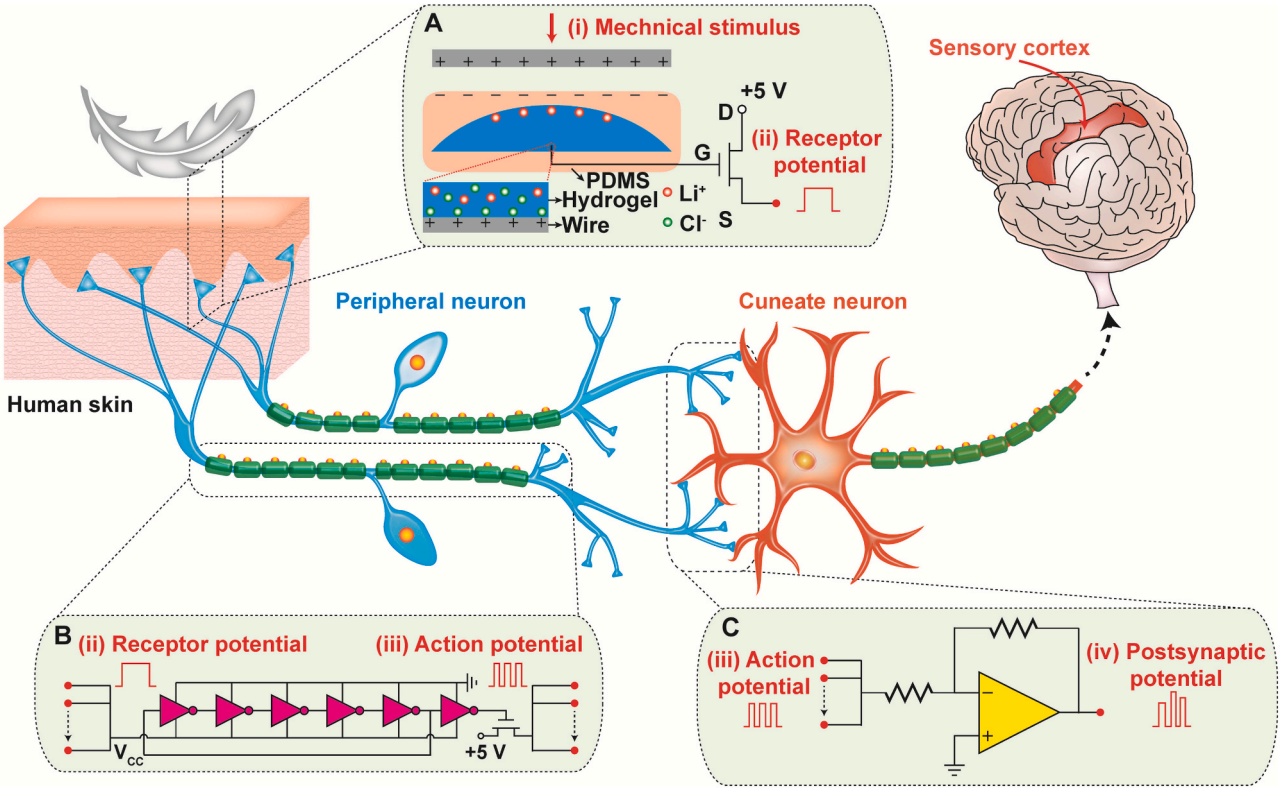


**Fig. 1.** Schematic illustration of a bioinspired artificial SA-I tactile afferent nervous system. A, A TMR as a SA-I mechanoreceptor. All the mechanoreceptors connected to one artificial peripheral neuron define a receptive field. B, A ring oscillator in combination with a transistor as an artificial peripheral neuron for spike generation. C, An inverting amplifier circuit as a synaptic structure containing multiple synapses of an artificial cuneate neuron.

hundreds of micrometres. The superior perception capability of the human fingertip is probably associated with the presence of four different mechanoreceptors and the role of overlapping of receptive-fields, and the parallel computing of data from a huge number of tactile receptors in the tactile nervous system which is the key to the fast sensoric response. The four mechanoreceptors are slowly adapting type I (SA-I), fast adapting type I (FA-I), slowly adapting type II (SA-II), fast adapting type II (FA-II) [20]. A receptive field comprises a certain number of the same type mechanoreceptors belonging to one tactile afferent nerve. The SA-I afferents that are equipped with the Merkel nerve endings fire spikes in response to stimuli with two distinct features. One feature is a continuous firing during stimulations. Another feature, which is more important, is the so-called the slowly adapting behaviour with a relatively high spike rate in the ramp phase at the beginning of a physical contact followed by a continuous decrease in rate overtime during the static phase [20]. Force-sensitive polymer films are commonly used for artificial tactile sensor arrays [16–18] typically to emulate the SA-I afferent. However, only the trait of a constant electric response during stimulations has been replicated thus far. The adapting feature of the SA-I afferents that is particularly beneficial to power saving in tactile perception is yet to realize. Moreover, the use of such a resistive sensor array is power inefficient as power supply is always needed for the sensors to respond to external stimuli and the resistive sensors dissipate non-negligible amounts of power even at their inactive state.

The superior perception capability of human hand is further associated with the unique signal processing mechanisms in biological tactile nervous systems. It has generally been attributed to neural activities in the cerebral cortex for a high-level extraction of geometric features of stimuli [21]. However, the latest studies on a limited number of biological somatosensory peripheral nerves suggest that the computation for extraction of geometric features starts at the level of the branched first-order tactile neurons in the tactile processing pathway [22,23]. How the tactile peripheral nervous systems (TPNSs) process and use tactile information remains to be confirmed. From the electronic engineering perspective, hardware deployment of artificial systems that emulate the biological TPNSs is significantly lagging behind the corresponding theoretical studies based on physiological experimental results.

Here, we report a hardware-based biomimetic artificial SA-I TPNS that is characterized by super-high response sensitivity and facilitates energy-efficient neuromorphic computation. The artificial SA-I TPNS is implemented simply by employing the well-established sensing method and circuit design. The design takes advantage of the structural features of the biological TPNS counterpart, i.e. the overlapped receptive fields in the skin, the arborization of the peripheral neurons and many-to-many synaptic connections between the peripheral neurons and the cuneate neurons (Fig. 1). A transducer based on triboelectric effects, i.e. triboelectric nanogenerator (TENG) [24–30], is connected to the gate electrode of a transistor. This implementation completes a circuit in analogue to a SA-I mechanoreceptor, i.e. the Merkel cell-neurite complex distributed superficially in the skin (Fig. 1A). This circuit is thus referred to as tribotronic mechanoreceptor (TMR) hereafter. A downstream ring oscillator in combination with a transistor is employed to approximate the function of the peripheral neuron for spike initiation (Fig. 1B). A simple inverting amplifier circuit is harnessed to emulate the synaptic structure containing multiple synapses, i.e. heterosynaptic structure (Fig. 1C). The TMR is supersensitive owning to its unique capability of responding to approaching objects prior to physical contact. It is self-powered during mechano-electric transduction through converting mechanical energy into electric signals. It further exhibits the slowly adapting feature of the SA-I mechanoreceptor, which is significantly beneficial to power efficiency. Hence, our artificial SA-I afferent nervous system represents an event-driven system and, mathematically, a typical convolutional neural network (CNN). In what follows in the remainder of this report, it is shown capable of delivering high-fidelity

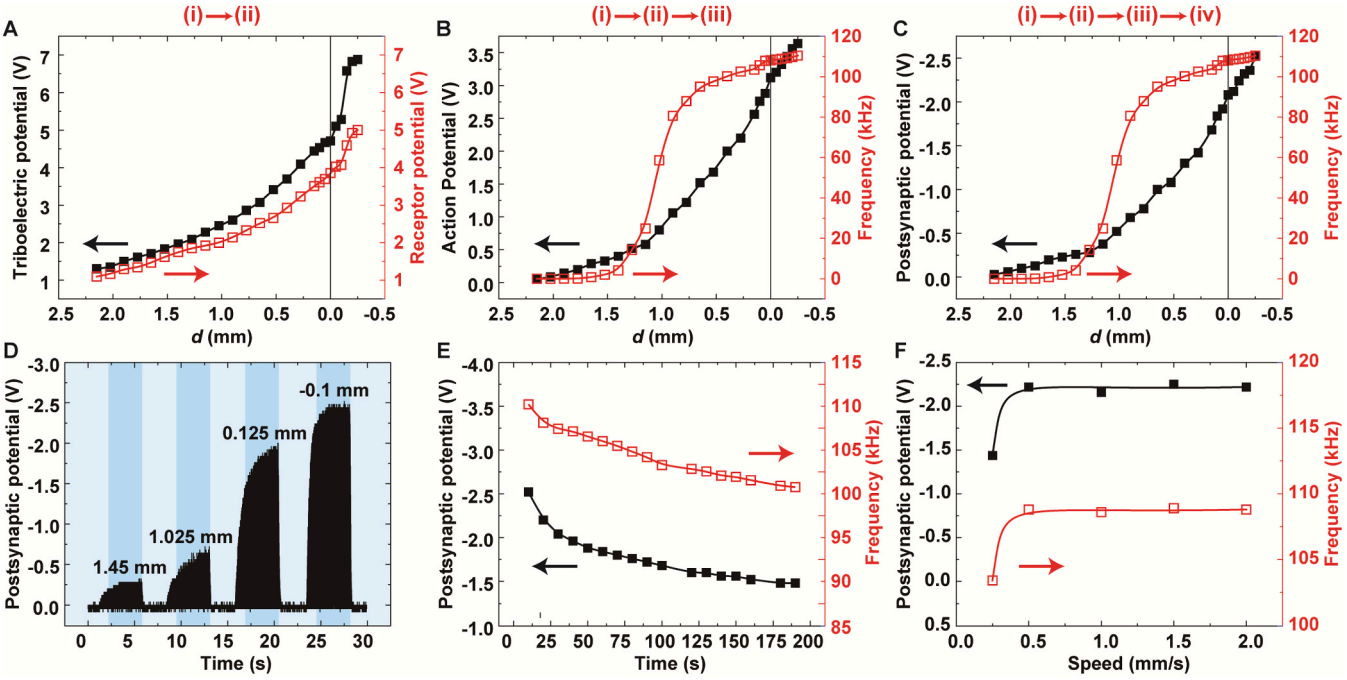


**Fig. 2.** Characteristics of the signal processing pathway in a one-branch artificial SA-I tactile afferent in response to mechanical stimuli. A, Variation of triboelectric potential and receptor potential with object-skin distance, *d*. The $d < 0$ region represents the skin deformation phase resulting from the physical object-skin contact at different degrees. B, Variation of magnitude (left axis) and frequency (right axis) of the action potential (i.e. the output voltage of the ring oscillator) with *d*. C, Variation of magnitude and frequency of the postsynaptic potential with *d*. D, Temporal development of postsynaptic spike trains at different *d*. Dark blue regions indicate the time intervals during which the object is in sojourn with the skin at the given *d*. E, Time evolution of magnitude and frequency of the postsynaptic potential during the static contact phase at $d = -0.250$ mm. F, Variation of magnitude and frequency of the postsynaptic potential with the motion speed of the object towards the skin. All experimental results in A to C were obtained from fresh contact events by moving the object from afar towards the artificial skin to a specific distance at a speed of 2 mm/s. (For interpretation of the references to colour in this figure legend, the reader is referred to the web version of this article.)

map of force distribution with a minimum resolvable dimension 2 times smaller than that of the aforementioned state-of-the-art electronic skins, i.e., the minimum inter-receptor distance.

## 2. Experimental section

### 2.1. Fabrication of arrayed tribotronic mechanoreceptors

An array of holes in a layer of tape was prepared using cutter plotter (Graphtec, Craft ROBO ProS). The diameter of the holes and the distance between the centres of the nearest neighbouring holes were 2.5 mm and 5 mm, respectively. The tape was then pasted on a substrate (glass or Acrylic) as a mask for the preparation of hydrogel droplet arrays. A bundle of metallic wires was covered by the mask. Each wire was allocated to a hole and insulated from one another.

Polyacrylamide (PAAm) hydrogel containing lithium chloride (LiCl) was employed as the ionic conductive PAAm-LiCl hydrogel. The LiCl, acrylamide, ammonium persulfate, N,N′-methylenebisacrylamide, N,N,N′,N′-tetramethylethylenediamine and Sylgard™ 184 silicone elastomer were used as received from Sigma-Aldrich. The PAAm-LiCl hydrogel solution was prepared by dissolving acrylamide powder (14 wt% relative to deionized water) into a 8 M LiCl aqueous solution. Subsequently, ammonium persulfate (0.17 wt%), N,N′-methylenebisacrylamide (0.06 wt%) and N,N,N′,N′-tetramethylethylenediamine (0.25 wt%), with respect to the weight of acrylamide, were consecutively dissolved in the solution. Then, the solution was transferred by pipette into the prepared hole array of the tape mask on the substrate and incubated in an oven at 50 °C for 1 h to form the PAAm-LiCl hydrogel droplets. The height of the hydrogel droplets was controlled by the solution volume. In each hole, the hydrogel drop was electrically connected to an embedded wire.

For the preparation of a polydimethylsiloxane (PDMS) film, the base and curing agent of Sylgard™ 184 silicone elastomer were mixed in a 10:1 wt ratio. After degassing in a vacuum oven at room temperature, the elastomer mixture was evenly coated on the surface of the hydrogel droplet array and then cured at 80 °C for 10 h to form a uniform PDMS film of thickness about 2 mm (Fig. S1). The PDMS film would later serve as the friction layer for triboelectrification, while the Al plates used for contact were made of Al foils attached to acrylic substrates in different sizes. The Al rod was prepared by wrapping a stain steel rod with an Al foil.

### 2.2. Preparation of electronic circuit

A printed circuit board (PCB) was designed to construct the two-tier tactile nervous system (Supplementary Fig. S2). All electronic parts were purchased from *Farnell*. The PCB board was divided into two parts. The first part imitated the first-order neurons, including the tribotronic transistors to imitate the function of the SA-I mechanoreceptors and the ring oscillators to imitate the nerve fibres, which were gated by the triboelectric potential and powered by $V_{DD}$. The second part with inverting amplifier arrays imitated the synaptic structures of the second-order neurons. It integrated action potentials from the connected first-order neurons and powered by $V_{S+}$ and $V_{S-}$. The two parts were connected via DuPont lines to construct the patterns of divergence and convergence of the first-order neurons onto the second-order neurons.

### 2.3. Characterization of our artificial SA-I tactile neuron

A piece of aluminium foil attached to an acrylic plate was used as the mobile object (denoted Al plate) in the whole measurement process unless otherwise specified. A programmable linear motor (Zaber Technologies T-LSR300B) was used to precisely control the movement (relative displacement, speed and acceleration) of the mobile Al plate.

The Al plate was mounted on the mobile terminal of the linear motor, while the mechanoreceptor array was fastened on the fixed terminal. A power supply was connected to the circuit to maintain $V_{DD} = 5$ V, $V_{S+} = +10$ V and $V_{S-} = -10$ V. All of the measurements were performed in an ambient environment at room temperature.

To investigate the distance-dependent output of the one-branch artificial afferent, the Al plate was driven to approach to the PDMS film. It was stopped at a predetermined distance from the surface of the PDMS film and stayed still for 10 s to record the electrical output signals. Then, it was brought back to its original position to complete a test cycle. The triboelectric and receptor potentials were measured using a high-precision Semiconductor Parameter Analyzer (Agilent Technologies, B1500A). The action potential and postsynaptic potential were recorded using an oscilloscope (Siglent, SDS 1102CML). For the slowly-adapting-behaviour characterization, the postsynaptic potential was recorded every 10 s for a total period of 190 s during which the Al plate and the PDMS film were in physical contact. For the dynamic characterization, the Al plate was made to move at different speed from 0.25 to 2 mm/s towards the PDMS film to investigate the influence of speed on the postsynaptic signal. For characterizing the synaptic circuit, the Al foil was attached to the surface of a PDMS hemisphere that was in turn fixed on the linear motor and driven to become in contact with the PDMS film. Around the contact point, three mechanoreceptors differently distanced from the Al plate were chosen to record their respective postsynaptic potential. The integrated postsynaptic potential was registered at the same time using a four-channel oscilloscope (RIGOL, DS4054). In the characterization of the two-tier neuron network, the 16 second-order neurons were divided into four groups and the same movement of the Al plate was repeated four times to enable recording of all the post-synaptic potentials using the four-channel oscilloscope (RIGOL, DS4054).

## 3. Results and discussion

The TMR comprises primarily a conductive hydrogel droplet connected to the gate terminal of an n-channel enhancement type field-effect transistor shown in Fig. 1A. The conductive hydrogel droplets containing $Li^+$ and $Cl^-$ ions are embedded in soft polydimethylsiloxane (PDMS) film, hereby referred to as an artificial skin. An object composed of ordinary materials tends to be positively charged when getting a physical contact with a PDMS film as a result of triboelectric effect [31]. When the object approaches the artificial skin, a displacement current arising due to the change of the polarization associated with the electrostatic surface charge is generated. This current leads to a positive triboelectric potential on the transistor's gate terminal (Fig. S5) [32]. Consequently, the transistor is turned on and a receptor potential is generated at its source terminal (Fig. 1A). The receptor potential is retained during the object-skin interaction. Aluminium (Al), glass, Kapton and paper were used as representative objects of distinct materials for generating the mechanical stimulations for experiment. Results with an Al plate as the object are presented throughout this report.

To understand how our artificial SA-I TPNS processes tactile information in the signal pathway, a one-branch artificial SA-I TPNS is first characterized. This system comprises one TMR, one artificial peripheral neuron and one synaptic structure, all of which are sequentially interconnected (Fig. 2). The triboelectric potential and the receptor potential in the TMR already start to change when the approaching Al plate is at a distance ($d$) around 2.2 mm away from the artificial skin as shown in Fig. 2A. The spatial position where the plate starts to get in physical contact with yet causes no deformation to the artificial skin is defined as $d = 0$. Thus, any position with $d \geq 0$ belongs to the approaching phase. The magnitude of both potentials is seen to increase monotonically with decreasing $d$. This early warning capability is unique and superior to the force-sensitive polymers as artificial skin that relies on the transduction mechanism of skin deformation. How the triboelectric potential is correlated to $d$ can be well understood by referring to the first-principles theory of the extended Maxwell equations [32]; our theoretical analysis indeed agrees well with the experimental result (Fig. 2A vs. Fig. S3B). The increase in both triboelectric and receptor potential proceeds upon physical contact between the Al plate and the skin ($d = 0$) and it experiences an acceleration with negative $d$ ($d \leq 0$). This physical contact phase with $d \leq 0$ represents the degree of deformation of the artificial skin ($|d|$), largely resembling the tissue deformation in the human skin. The pressure at $d = -0.250$ mm is found to be ~50 kPa (Fig. S4), which is comparable to light touching and tapping by a human hand. Surface charge density of the object is obtainable from the receptor voltage at $d = 0$ as seen in Fig. S3B, demonstrating the capability of perceiving the object surface properties using our artificial SA-I TPNS.

The receptor potential is then fed to the ring oscillator in the artificial peripheral neuron to initiate pulses at the drain terminal of the downstream transistor right after the ring oscillator (Fig. 1B). The generated pulses are analogue to action potentials or a spike train fired at the SA-I peripheral neurons although there are subtle differences in, e.g. shape and frequency. For simplicity, we refer the pulses generated by the ring oscillator as action potential or spikes in this work. The action potential increases monotonously both in magnitude and oscillation frequency with decreasing $d$ (Fig. 2B). In the approaching phase, the sensitivity defined by the slope of the frequency-distance relation is maximized at $d \approx 1.1$ mm, representing an excellent early warning capability of our artificial skins. The frequency of the action potential of our artificial neuron changes nonlinearly with $d$, which essentially follows the dependence of the firing rate on skin displacement for the biological SA-I afferents [33,34].

The action potential propagates to the inverting amplifier circuit and generates the output referred to as the postsynaptic potential. This postsynaptic potential is seen in Fig. 2C akin faithfully to the action potential in both magnitude and frequency for their dependency on $d$. The high fidelity in signal propagation through the inverting amplifier circuit as in a synaptic structure is, hence, evident. The spike trains in response to four individual contact events are registered in Fig. 2D. During a static contact at a fixed $d$, both magnitude and frequency of the postsynaptic potential decrease gradually over time (Fig. 2E and Fig. S6). The time span for the postsynaptic potential to drop from its peak (at $t = 0$) to the normal low level, i.e. adaptive behaviour, is ~3 min. It can be readily reduced to ~100 ms by appropriate circuit adjustment (Fig S7). Therefore, the featured slowly adapting behaviour of the biological SA-I afferent [4,20] has, for the first time, been reproduced using our TMRs. The slowly adapting response is beneficial to power saving in tactile perception, in particular, when a robotic hand or a prosthetic hand grasps and holds an object.

The temporal feature of the postsynaptic potential in response to dynamic stimuli further reveals that the response during the approaching phase is dependent on the motion speed (more data in Fig. S8). When examining the motion speed-dependence of frequency (Fig. 2F), the frequency during the contact phase appears insensitive to the motion speed although the frequency at 0.25 mm/s is ~6% lower than those with the motion speed $\geq 0.5$ mm/s. Therefore, the responsive feature of our artificial SA-I afferent nerve in the contact phase is, to great extent, analogue to the biological SA-I afferent nerve in that the frequency is mainly sensitive to the intensity of mechanical stimuli [20]. However, our artificial afferent nerve is exclusive in that its unique dependence of the response on the motion speed during the approaching phase can be exploited for discerning the dynamic feature of stimuli.

Our artificial SA-I afferent nerves represent an event-driven system. The power consumption of a representative system consisting of a mechanoreceptor and an artificial peripheral neuron is below 15 nW at the inactive state, i.e. without mechanical stimuli, and 28.6 mW at the active state (Fig. S9). For an event-driven system with sparse activations as a biological TPNS, the power consumption at the inactive state is crucial. The inactive-state power consumption is nearly 600 times lower than that of a similar artificial nerve with a resistive mechanoreceptor and an organic ring oscillator (*16*). The ultralow power consumption at

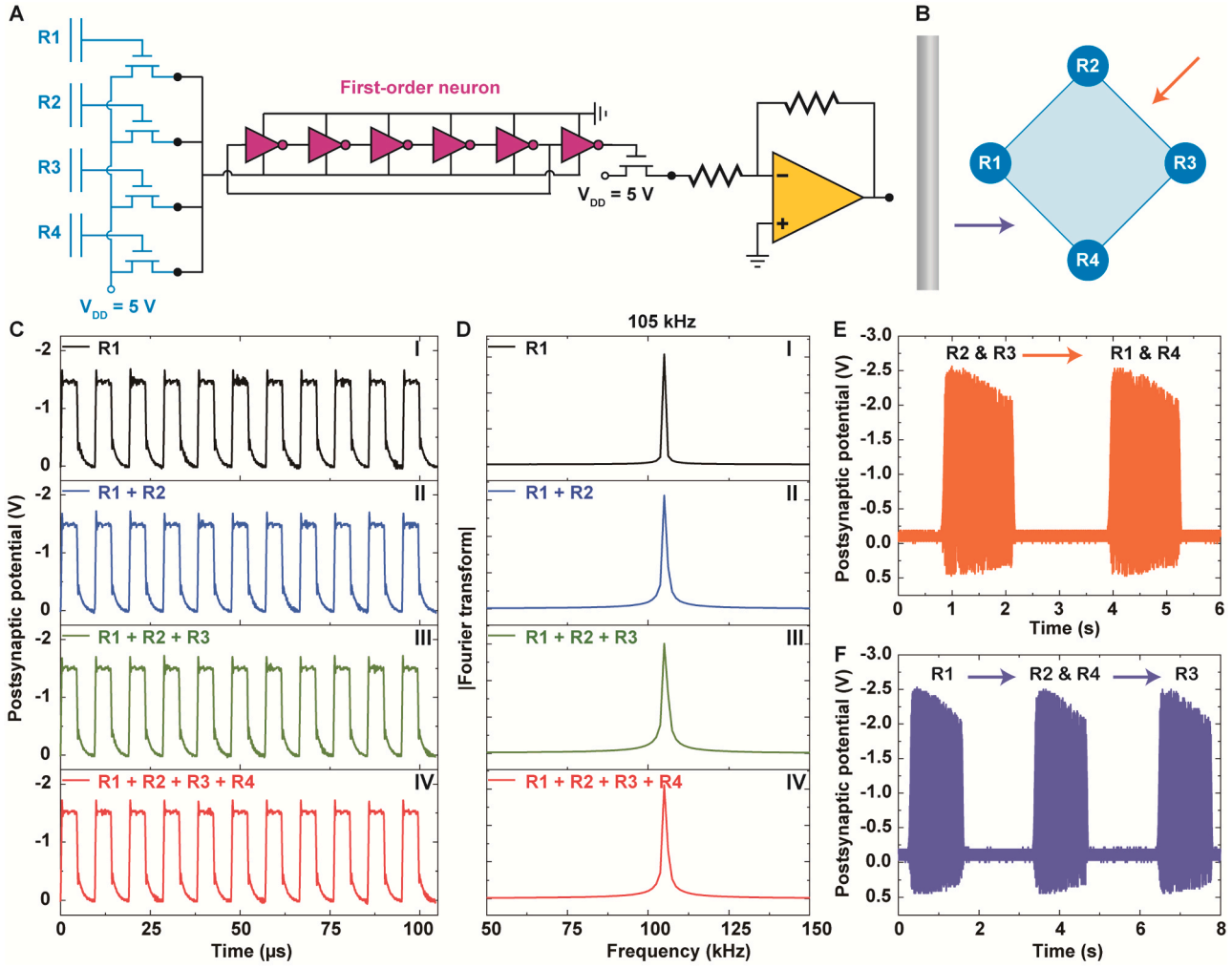


**Fig. 3.** Characteristics of an artificial SA-I tactile afferent distally branched with four mechanoreceptors. A, Configuration of the artificial tactile afferent nerve comprising 4 receptors (labelled R1 to R4) connected in parallel to one artificial peripheral (first-order) neuron and then one synapse. B, Spatial layout of the 4 TMRs for direction recognition of a moving Al rod (silver vertical bar) in two different directions indicated by the arrows. C, Invariant postsynaptic potential of the tactile afferent when stimulating different TMRs and their combinations. D, Fourier transform of the signals in C also showing an invariant frequency upon stimulating differently combined mechanoreceptors. E-F, Varied number of spike trains, postsynaptic potential, when moving the rod in the two directions in B. (For interpretation of the references to colour in this figure legend, the reader is referred to the web version of this article.)

its inactive state stems from the self-power characteristic of the transduction and the very low off-state current of the transistor. Generally, the total power consumption at an active state is the sum of the power consumed in the sensing operation of the transducer ($P_s$) and the power consumed in the downstream neuromorphic circuit ($P_c$). The latter, $P_c$, can be efficiently reduced to a very low level by careful circuit design implemented by means of the advanced semiconductor chip technology [35]. The former, $P_s$, can, thus, dominate the total power reduction and it increases with the number of sensors. The transducer employed here directly converts mechanical energy from external stimuli to electrical signal, i.e. self-powered, thereby ruling out the need of external power supply for transduction. Therefore, the design of our artificial SA-I TPNS is uniquely scalable for practical applications in neurorobotics and neuroprosthetics.

The extraordinary perception capability of the human skin is in part associated with the distal axon of the tactile peripheral neurons that branches in the skin with a number of mechanoreceptors, thereby yielding complex receptive fields on the skin [22,34,36]. It has been found that the spatial layout of the receptive fields constitutes a mechanosensory encoding mechanism that allows for individual neurons to signal tactile information containing spatial details of touch objects [22,34]. In order to emulate such key functions, an artificial SA-I afferent nerve featuring four TMRs connected in parallel to one artificial peripheral neuron, i.e. a ring oscillator with a transistor, and then to one synapse structure, i.e. an inverting amplifier circuit (Fig. 3A) is constructed. The four TMRs are arranged in a rectangle form of an artificial skin (Fig. 3B).

The spike trains show the same characteristics when different numbers of the TMRs are recruited in a contact event (Fig. 3C). Upon Fourier transform of the spike trains, the frequency is found invariant when different combinations of the mechanoreceptors are stimulated (Fig. 3D). This spike firing property allows for movement recognition with the simple arrangement of the TMRs in a rectangle. When an object, an Al rod in this specific case, moves across the receptive field at different speeds and in different directions (Fig. 3B), the recorded sequential firing trains show similar features, but with different numbers of the spike trains in different moving directions (Fig. 3E and F). When the rod moves from the upper right to the lower left (orange arrow in Fig. 3B), two sets of TMRs (R2&R3 and R1&R4) are sequentially involved. When it moves along the horizontal direction (blue arrow), three sets of TMRs (R1, R2&R4 and R3) are sequentially recruited. The speed of the Al rod movement over the receptive field can be discerned by the temporal length or the interval of the individual spike trains fired when one TMR or a subset of TMRs is recruited during the object-skin

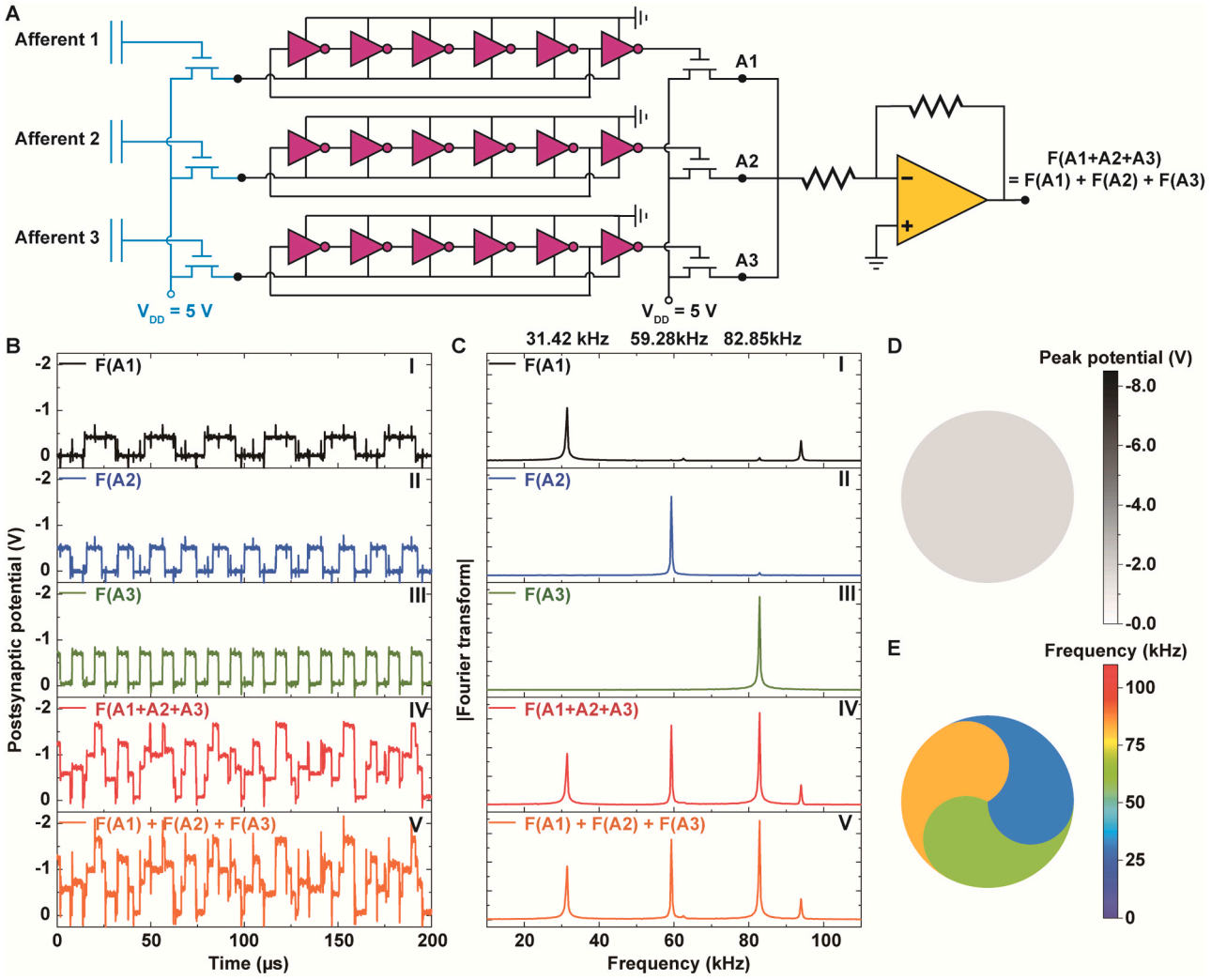


**Fig. 4.** Characteristics of a triple-synaptic integration. A, Configuration of the artificial tactile afferent comprising three artificial peripheral (first-order) neurons connected to a common synaptic structure for a hetero-synaptic integration. B, Postsynaptic potential for individual (I-III) and integrated (IV) synapses. C, Fourier transform of the signals in B. D, Peak voltage of the integrated postsynaptic potential equal to the sum of the peak voltages of the individual artificial first-order neurons. E, Preserved frequencies of the stimulated individual artificial first-order neurons when examining the integrated postsynaptic potential.

interaction.

Previous neurobiological studies indicate that a cuneate neuron receives signals from an ensemble of cutaneous afferents (~300) [37]. A multiple-synaptic integration of tactile information from a cohort of peripheral neurons is indeed important for the rapid classification of tactile information at the level of the cuneate neuron by the temporal-to-spatial conversion in the somatosensory pathways [4,22,23]. Use of an inverting amplifier circuit as the synaptic structure is shown to perform the spatial summation of multiple-synaptic signals as evidenced in Fig. 4. Different from the configuration in Fig. 3A, three artificial peripheral neurons, each connected to one TMR, are linked to their respective synaptic structure of inverting amplifier circuit (Fig. 4A). The mechanoreceptor-object distance from an approaching Al plate to the three TMRs in the PDMS film is mostly different over time of the movement. Although the difference in distance is small, it is sufficient to generate distinct action potential signals from the three artificial peripheral neurons, denoted as **A**1, **A**2 and **A**3. The postsynaptic potentials, resulting from the transition of an individual action potential through a synapse of inverting amplifier circuit, are, then, detected (see Method in Supporting Information) and denoted as **F**(**An**) (n = 1, 2 and 3). Here, **F** represents the operation of the synapse of inverting amplifier circuit. The final magnitude and frequency of **F**(**An**) are displayed in Fig. 4B and C, respectively. When the action potentials from the three TMRs are integrated at one synapse of inverting amplifier circuit in the system as illustrated in Fig. 4A, the result is the integration of A1, A2 and A3, i.e. **F**(A1+A2+A3) (Fig. 4B-IV). **F**(A1+A2+A3) is essentially equal to the sum of the individual postsynaptic potentials, **F**(A1)+**F**(A2)+**F**(A3) (Fig. 4B-V). Consistently, the frequency components of **F**(A1+A2+A3) in Fig. 4C-IV are identical to those of **F**(A1)+**F**(A2)+**F**(A3) in Fig. 4C-V. By merely examining the magnitude of the postsynaptic potential (Fig. 4D), it is challenging to distinguish the number of artificial peripheral neurons evoked. In contrast, the postsynaptic potential of our artificial tactile afferent can faithfully deliver the frequency components in the tactile signal from the stimulated artificial peripheral neurons (Fig. 4E). The frequency information is an added dimension and it allows one to discern the number of the stimulated artificial peripheral neurons. This characteristic is analogue to the fire-rate coding exploited in biological nervous systems. However, it is unfeasible to rely on a single synapse to distinguish the spatial information of the artificial peripheral neurons evoked in response to a stimulus. Invoking a nervous system containing overlapped receptive fields and multiple synaptic structures can resolve the problem.

In an anatomical somatosensory system, tactile information collected in the peripheral nervous system comprising the peripheral neurons,

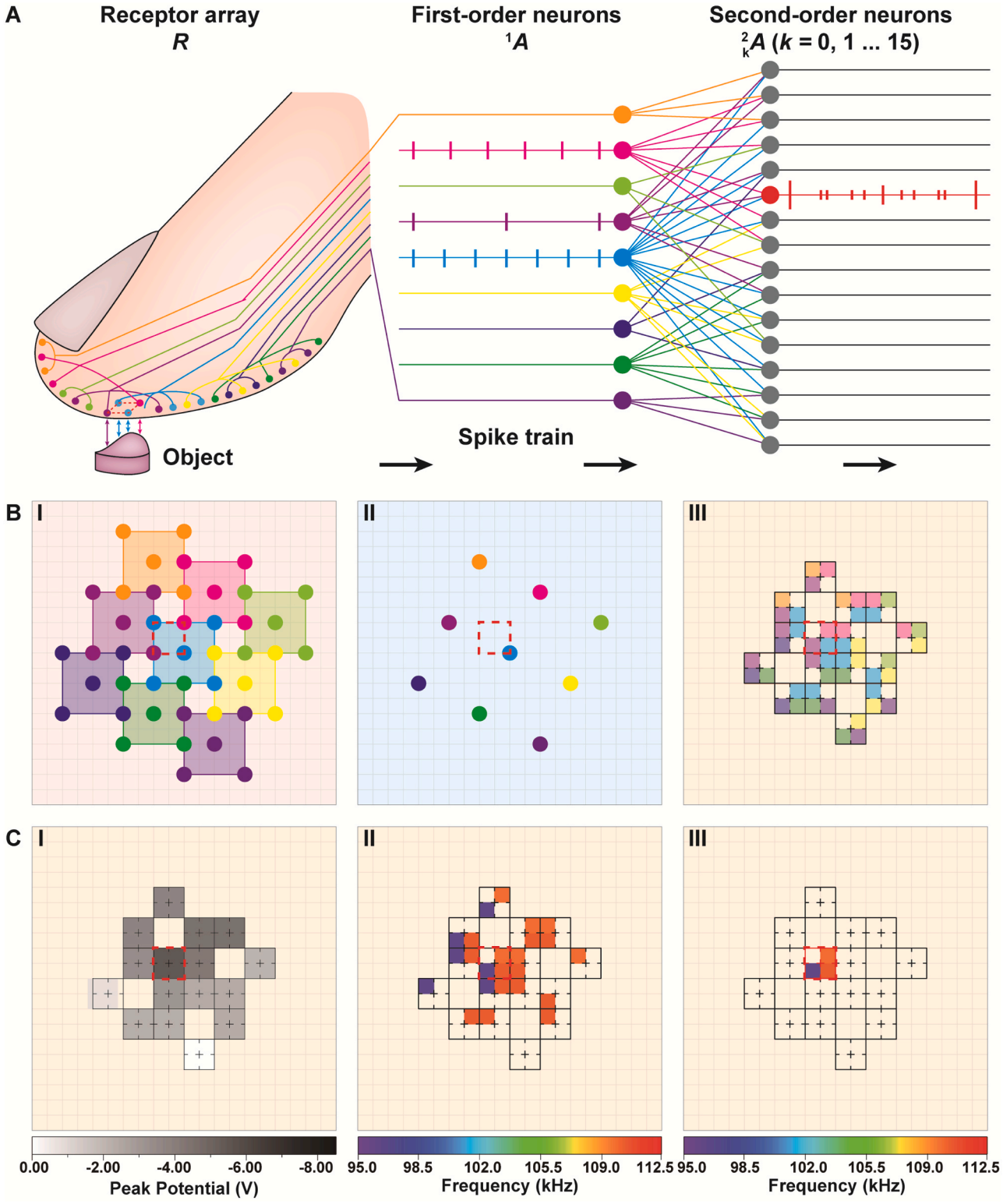


**Fig. 5.** Spatial recognition of a two-tier artificial SA-I TPNS in response to a mechanical stimulus. A, Schematic nervous system for neuromorphic signal classification comprising an input layer of 45 TMRs (*R*) distributed in the PDMS skin, the first convolution layer of 9 artificial first-order neurons ($^1A$) and the second convolution layer containing 16 synaptic structures of the second-order neurons ($^2_kA$ ($k$ = 0,1,2…15)). B, Spatial layout of the mechanoreceptors (I) being mapped to the artificial first-order neurons (II) and the synaptic structures (III). C, Spatial maps of the ensemble of postsynaptic potentials in magnitude (I) and frequency (II) showing that the frequency coding can provide a precise place code with an improved spatial resolution to the contact event (III). In C(III), the colours in the three blocks are different. The area of the stimulus is indicated in the dashed squares. (For interpretation of the references to colour in this figure legend, the reader is referred to the web version of this article.)

also called the first-order neurons, is transmitted to the second- and then third-order neurons in the central nervous system. The anatomical arborization of neurons allows their distal dendrites and proximal axon terminals for complex synaptic connections to the lower and higher-order neurons (Fig. 1). The structure of divergence and convergence of the first-order neurons onto the second-order neurons allows the second-order neurons to encode a great amount of different spike patterns of the first-order neurons [4]. The structural features of the tactile afferent nervous system have motivated the design of a two-tier artificial TPNS that can perform fast tactile signal processing for extraction of geometric features (Fig. 5A). The structure of this hardware demonstrator is described in Supplementary Information. Briefly, it comprises three consecutively interconnected layers, i.e. 45 TMRs, 9 artificial first-order (peripheral) neurons and 16 synaptic structures of artificial second-order neurons (Fig. S8 and 9). Each artificial peripheral neuron is connected in parallel to five TMRs, defining a receptive field. With each colour representing a specific receptive field, Fig. 5B illustrates the distribution of the TMRs (I), the mapping of the TMRs to the artificial peripheral neurons (II) and subsequently to the synaptic structures (III). Each block having three mosaics of different colours and one blank in Fig. 5B-III represents one synaptic structure. It has previously been suggested by theoretical simulations that the functional overlap of different receptive fields is likely critical for an enhancement of spatial resolution [34,36]. In our design, the receptive field of each artificial peripheral neuron can overlap with four neighbouring receptive fields at its corners, as shown in Fig. 5B-I.

To characterize the spatial recognition and the recognition resolution of our artificial TPNS, the ensemble of postsynaptic potentials is studied for their collective and collaborative responses to a mechanical stimulus made by contacting the system with a small Al plate (Fig. 5A-left). This Al plate is 5 mm in size, which is half of the receptive field size and also equal to the minimal inter-receptor distance. When the Al plate is brought to physical contact with the artificial skin ($d \leq 0$) with the contact area marked by the dashed lines in Fig. 5A–C, all the TMRs that are in interaction with the plate are recruited for the generation of receptor potential. The recruited TMRs evoke the downstream artificial first-order neurons dyed with blue, pink and purple for spike firing (Fig. 5A-middle). The inputs from the evoked artificial first-order neurons are integrated at the synaptic structures in a way similar to the biological somatosensory pathway [4,22]. The signal integration thereby results in distinct output patterns (maps) of the ensemble of postsynaptic potentials in peak magnitude (Fig. 5C-I) and frequency components (Fig. 5C-II).

Although using frequency coding in an artificial afferent nerve with a single synapse can preserve the frequency components of the input from the multiple artificial first-order neurons, it cannot provide the spatial distribution of the recruited TMRs as analysed earlier (Fig. 4). This limitation can be readily mitigated through frequency coding by exploiting an intrinsic feature of our design of the artificial TPNS, i.e. two neighbouring artificial second-order neurons share two TMRs connected to their respective artificial first-order neurons (Fig. 5B). The achieved spatial distribution of the frequency components corresponding to the recruited TMRs in the ensemble of postsynaptic signals is shown in Fig. 5C-II. The function of this structural feature of our artificial TPNS design may provide a clue about how a biological TPNS functions. Furthermore, it is evident that only one block that corresponds precisely to the contact area contains three distinct frequencies. This block can be readily selected by implementing a threshold operation that one artificial second-order neuron fires spikes only when it receives signals simultaneously from all the three artificial first-order neurons it connects to (Fig. 5A-right). As a result, the geometric information about object-artificial skin interaction has a spatial resolution of 2.5 mm. This value is 4.5 times smaller than the distance between the centres of two nearest neighbouring receptive fields (11.2 mm) and 2 times smaller than the smallest inter-receptor distance (5 mm). It is worth noting that this threshold operation is equivalent to the coincidence detection that is one of the most fundamental computational mechanisms of a brain, i.e. the central neurons preferentially respond when receiving synchronous inputs from many sources [4, 38–41]. A recent study on biological tactile afferent suggests that a coincidence detector likely works very early in the distal peripheral nervous networks, at the level of first-order neurons [22]. The signal processing of our artificial TPNS is thus in consistency with this assumption made in the neurobiological study. The neural connectivity and the neuromorphic signal processing of our artificial TPNS can be mathematically modelled with a convolutional neural network (CNN) comprising an input layer and two convolutional layers, represented by a $9 \times 9$ matrix for $\boldsymbol{R}$, a $3 \times 3$ matrix for ${}^{1}\boldsymbol{A}$ and a series of $k_2^A$ values ($k = 0,1,2\ldots15$) (Fig. S10 and the description in Supplementary Information). Through the two convolution layers, the tactile image from the mechanoreceptor array is successfully transmitted to a group of 16 feature maps (i.e. place codes). These features become the input to the downstream artificial neurons in analogue to the third-order neurons ending at the somatosensory cortex to perform the higher-level classification of the tactile information associated with the conscious perception of sensation.

## 4. Conclusion

In summary, we have presented an artificial TPNS with self-powered transducers that potentially advances the electronic skin technology. With the mechanoreceptors we have designed, the slowly adapting feature of the biological SA-I afferent has been well reproduced. This slowly adapting behaviours, in combination with the event-driven working manner and parallel information processing with spikes, leads to the scalability of our artificial TPNS, i.e., the number of receptors and artificial neurons increase without causing an appreciable increase in the latency and power consumption. The artificial TPNS processes tactile signals which can be described using the CNN model. By combining the design of overlapped receptive fields, our artificial TPNS delivers high-fidelity tactile information with the resolvable dimension two times smaller than the minimal inter-receptor distance. Therefore the barrier that limits the spatial resolution of the existing electronic skin technologies in mapping tactile stimulation has been broken. This result has opened up a route for artificial skins towards the exceptional capability of human fingertips in discriminating fine textures. Although simple hardware architecture with well-known circuit design to emulate the neural structure has been used, the results of tactile perception are profound. Following the conceptual approach for hardware design, remarkable advancements towards attaining the superior function of the natural tactile nervous system are expected provided that the advanced semiconductor chip technology and circuit technology (e.g., application specific integrated circuits, ASICs) are exploited.

## CRediT authorship contribution statement

L.B.C. proposed the concept, designed circuits, fabricated and measured the samples, analysed data, prepared figures and references drafting and wrote part of the initial draft. C.Y.W. assisted in circuit design. Z.L.W. and S.L.Z. provided critical feedback to improvement of the manuscript. S.L.Z. made critical revision of the manuscript. Z.B.Z. provided critical feedback to operation principles, device concept, circuit fabrication, data interpretation and neural network, wrote the initial draft and provided critical revision of the article.

## Declaration of Competing Interest

The authors declare that they have no known competing financial interests or personal relationships that could have appeared to influence the work reported in this paper.

## Acknowledgements

The authors would like to thank Dr Wei Xia for assistance in the pressure-deformation measurement and Dr Chi Zhang and Dr Junqing Zhao for helpful discussion. This work was mainly supported by the faculty fund of Uppsala University, Sweden.

## Appendix A. Supporting information

Supplementary data associated with this article can be found in the online version at doi:10.1016/j.nanoen.2020.105680.

## References

[1] C. Bartolozzi, L. Natale, F. Nori, G. Metta, Robots with a sense of touch, Nat. Mater. 15 (2016) 921–925, https://doi.org/10.1038/Nmat4731.
[2] K.W. Horch, G.S. Dhillon, Neuroprosthetics: Theory and Practice, World Scientific, 2004.
[3] D. Borton, S. Micera, J.D. Millan, G. Courtine, Personalized neuroprosthetics, Sci. Transl. Med. 5 (2013), 210rv2, https://doi.org/10.1126/scitranslmed.3005968.
[4] R.S. Johansson, J.R. Flanagan, Coding and use of tactile signals from the fingertips in object manipulation tasks, Nat. Rev. Neurosci. 10 (2009) 345–359, https://doi.org/10.1038/nrn2621.
[5] V.G. Macefield, R.S. Johansson, Control of grip force during restraint of an object held between finger and thumb: responses of muscle and joint afferents from the digits, Exp. Brain Res. 108 (1996) 172–184, https://doi.org/10.1007/BF00242913.
[6] C. HagerRoss, R.S. Johansson, Nondigital afferent input in reactive control of fingertip forces during precision grip, Exp. Brain Res. 110 (1996) 131–141, https://doi.org/10.1007/BF00241382.
[7] M. Dimitriou, B.B. Edin, Discharges in Human muscle receptor afferents during block grasping, J. Neurosci. 28 (2008) 12632–12642, https://doi.org/10.1523/Jneurosci.3357-08.2008.
[8] S. Furber, Large-scale neuromorphic computing systems, J. Neural Eng. 13 (2016), 051001, https://doi.org/10.1088/1741-2560/13/5/051001.
[9] W.Z. Wu, X.N. Wen, Z.L. Wang, Taxel-addressable matrix of vertical-nanowire piezotronic transistors for active and adaptive tactile imaging, Science 340 (2013) 952–957, https://doi.org/10.1126/science.1234855.
[10] C.M. Boutry, M. Negre, M. Jorda, O. Vardoulis, A. Chortos, O. Khatib, Z.N. Bao, A hierarchically patterned, bioinspired e-skin able to detect the direction of applied pressure for robotics, Sci. Robot 3 (2018), eaau6914, https://doi.org/10.1126/scirobotics.aau6914.
[11] C. Pang, G.Y. Lee, T.I. Kim, S.M. Kim, H.N. Kim, S.H. Ahn, K.Y. Suh, A flexible and highly sensitive strain-gauge sensor using reversible interlocking of nanofibres, Nat. Mater. 11 (2012) 795–801, https://doi.org/10.1038/NMAT3380.
[12] Y.C. Lai, J. Deng, R. Liu, Y.C. Hsiao, S.L. Zhang, W. Peng, H.M. Wu, X. Wang, Z. L. Wang, Actively perceiving and responsive soft robots enabled by self-powered, highly extensible, and highly sensitive triboelectric proximity- and pressure-sensing skins, Adv. Mater. 30 (2018), 1801114, https://doi.org/10.1002/Adma.201801114.
[13] C. Chi, X.G. Sun, N. Xue, T. Li, C. Liu, Recent progress in technologies for tactile sensors, Sensors 18 (2018) 948, https://doi.org/10.3390/S18040948.
[14] X. Pu, M.M. Liu, X.Y. Chen, J.M. Sun, C.H. Du, Y. Zhang, J.Y. Zhai, W.G. Hu, Z. L. Wang, Ultrastretchable, transparent triboelectric nanogenerator as electronic skin for biomechanical energy harvesting and tactile sensing, Sci. Adv. 3 (2017), e1700015, https://doi.org/10.1126/sciadv.1700015.
[15] J. Tao, R.R. Bao, X.D. Wang, Y.Y. Peng, J. Li, S. Fu, C.F. Pan, Z.L. Wang, Self-powered tactile sensor array systems based on the triboelectric effect, Adv. Funct. Mater. 29 (2019), 1806379, https://doi.org/10.1002/Adfm.201806379.
[16] Y. Kim, A. Chortos, W.T. Xu, Y.X. Liu, J.Y. Oh, D. Son, J. Kang, A.M. Foudeh, C. X. Zhu, Y. Lee, S.M. Niu, J. Liu, R. Pfattner, Z.N. Bao, T.W. Lee, A bioinspired flexible organic artificial afferent nerve, Science 360 (2018) 998–1003, https://doi.org/10.1126/science.aao0098.
[17] W.W. Lee, Y.J. Tan, H.C. Yao, S. Li, H.H. See, M. Hon, K.A. Ng, B. Xiong, J.S. Ho, B. C.K. Tee, A neuro-inspired artificial peripheral nervous system for scalable electronic skins, Sci. Robot 4 (2019), eaax2198, https://doi.org/10.1126/scirobotics.aax2198.
[18] S. Sundaram, P. Kellnhofer, Y.Z. Li, J.Y. Zhu, A. Torralba, W. Matusik, Learning the signatures of the human grasp using a scalable tactile glove, Nature 569 (2019) 698–702, https://doi.org/10.1038/s41586-019-1234-z.
[19] L. Skedung, M. Arvidsson, J.Y. Chung, C.M. Stafford, B. Berglund, M.W. Rutland, Feeling small: exploring the tactile perception limits, Sci. Rep. 3 (2013), https://doi.org/10.1038/Srep02617.
[20] R.S. Johansson, A.B. Vallbo, Tactile sensory coding in the glabrous skin of the human hand, Trends Neurosci. 6 (1983) 27–32, https://doi.org/10.1016/0166-2236(83)90011-5.
[21] S. Hsiao, Central mechanisms of tactile shape perception, Curr. Opin. Neurobiol. 18 (2008) 418–424, https://doi.org/10.1016/j.conb.2008.09.001.
[22] J.A. Pruszynski, R.S. Johansson, Edge-orientation processing in first-order tactile neurons, Nat. Neurosci. 17 (2014) 1404–1409, https://doi.org/10.1038/nn.3804.
[23] H. Jorntell, F. Bengtsson, P. Geborek, A. Spanne, A.V. Terekhov, V. Hayward, Segregation of tactile input features in neurons of the cuneate nucleus, Neuron 83 (2014) 1444–1452, https://doi.org/10.1016/j.neuron.2014.07.038.
[24] C. Zhang, W. Tang, L.M. Zhang, C.B. Han, Z.L. Wang, Contact electrification field-effect transistor, ACS Nano 8 (2014) 8702–8709, https://doi.org/10.1021/nn5039806.
[25] F. Xue, L.B. Chen, L.F. Wang, Y.K. Pang, J. Chen, C. Zhang, Z.L. Wang, $MoS_2$ tribotronic transistor for smart tactile switch, Adv. Funct. Mater. 26 (2016) 2104–2109, https://doi.org/10.1002/adfm.201504485.
[26] C. Zhang, Z.L. Wang, Tribotronics - a new field by coupling triboelectricity and semiconductor, Nano Today 11 (2016) 521–536, https://doi.org/10.1016/j.nantod.2016.07.004.
[27] L.B. Chen, F. Xue, X.H. Li, X. Huang, L.F. Wang, J.Z. Kou, Z.L. Wang, Strain-gated field effect transistor of a $MoS^2$-ZnO 2D–1D hybrid structure, ACS Nano 10 (2016) 1546–1551, https://doi.org/10.1021/acsnano.5b07121.
[28] S.W. Kim, K.J. Lee, Z.L. Wang, Nanogenerators and piezo/tribo-tronics, Nano Energy 61 (2019) 637–638, https://doi.org/10.1016/j.nanoen.2019.05.018.
[29] X. Pu, H. Guo, J. Chen, X. Wang, Y. Xi, C. Hu, Z.L. Wang, Eye motion triggered self-powered mechnosensational communication system using triboelectric nanogenerator, Sci. Adv. 3 (2017), e1700694, https://doi.org/10.1126/sciadv.1700694.
[30] X. Pu, Q. Tang, W. Chen, Z. Huang, G. Liu, Q. Zeng, J. Chen, H. Guo, L. Xin, C. Hu, Flexible triboelectric 3D touch pad with unit subdivision structure for effective XY positioning and pressure sensing, Nano Energy 76 (2020), 105047, https://doi.org/10.1016/j.nanoen.2020.105047.
[31] H.Y. Zou, Y. Zhang, L.T. Guo, P.H. Wang, X. He, G.Z. Dai, H.W. Zheng, C.Y. Chen, A.C. Wang, C. Xu, Z.L. Wang, Quantifying the triboelectric series, Nat. Commun. 10 (2019) 1427, https://doi.org/10.1038/S41467-019-09461-X.
[32] Z.L. Wang, On the first principle theory of nanogenerators from Maxwell's equations, Nano Energy (2019), 104272, https://doi.org/10.1016/j.nanoen.2019.104272.
[33] E.R. Kandel, J.H. Schwartz, T.M. Jessell, Do Biochemistry, M.B.T. Jessell, S. Siegelbaum, A. Hudspeth, Principles of neural science, McGraw-Hill, New York, 2000.
[34] D.R. Lesniak, K.L. Marshall, S.A. Wellnitz, B.A. Jenkins, Y. Baba, M.N. Rasband, G. J. Gerling, E.A. Lumpkin, Computation identifies structural features that govern neuronal firing properties in slowly adapting touch receptors, eLife 3 (2014), https://doi.org/10.7554/eLife.01488.
[35] B. Rajendran, A. Sebastian, M. Schmuker, N. Srinivasa, E. Eleftheriou, Low-power neuromorphic hardware for signal processing applications: a review of architectural and system-level design approaches, IEEE Signal Proc. Mag. 36 (2019) 97–110, https://doi.org/10.1109/MSP.2019.2933719.
[36] C.W. Eurich, H. Schwegler, Coarse coding: calculation of the resolution achieved by a population of large receptive field neurons, Biol. Cyber 76 (1997) 357–363, https://doi.org/10.1007/s004220050349.
[37] E.G. Jones, Cortical and subcortical contributions to activity-dependent plasticity in primate somatosensory cortex, Annu. Rev. Neurosci. 23 (2000) 1–37, https://doi.org/10.1146/annurev.neuro.23.1.1.
[38] P. König, A.K. Engel, W. Singer, Integrator or coincidence detector? The role of the cortical neuron revisited, Trends Neurosci. 19 (1996) 130–137, https://doi.org/10.1016/S0166-2236(96)80019-1.
[39] W.M. Usrey, The role of spike timing for thalamocortical processing, Curr. Opin. Neurobiol. 12 (2002) 411–417, https://doi.org/10.1016/S0959-4388(02)00339-2.
[40] J.J. Hopfield, Pattern-recognition computation using action-potential timing for stimulus representation, Nature 376 (1995) 33–36, https://doi.org/10.1038/376033a0.
[41] T. Masquelier, R. Guyonneau, S.J. Thorpe, Spike timing dependent plasticity finds the start of repeating patterns in continuous spike trains, PLoS One 3 (2008), e1377, https://doi.org/10.1371/journal.pone.0001377.